

ULTRAVIOLET SPECTROPOLARIMETRY WITH POLSTAR: CLUMPING AND MASS-LOSS RATE CORRECTIONS

KEN GAYLEY

Department of Physics and Astronomy, University of Iowa, Iowa City, IA, 52242

JORICK S. VINK

Armagh Observatory and Planetarium, College Hill, BT65 9DG Armagh, Northern Ireland

ASIF UD-DOULA

Penn State Scranton, 120 Ridge View Drive, Dunmore, PA 18512, USA

ALEXANDRE DAVID-URAZ

Department of Physics and Astronomy, Howard University, Washington, DC 20059, USA
Center for Research and Exploration in Space Science and Technology, and X-ray Astrophysics Laboratory, NASA/GSFC, Greenbelt, MD 20771, USA

RICHARD IGNACE

Department of Physics & Astronomy, East Tennessee State University, Johnson City, TN 37614, USA

RAMAN PRINJA

Department of Physics and Astronomy, University College London, Gower Street, London WC1E 6BT, UK

NICOLE ST-LOUIS

Département de physique, Université de Montréal, Complexe des Sciences, 1375 Avenue Thérèse-Lavoie-Roux, Montréal (Qc), H2V 0B3, Canada

SYLVIA EKSTRÖM

Department of Astronomy, University of Geneva, Chemin Pegasi 51, 1290 Versoix GE, Switzerland

YAËL NAZÉ

GAPHE, Univ. of Liège, B5C, Allée du 6 Août 19c, B-4000 Liège, Belgium

TOMER SHENAR

Anton Pannekoek Institute for Astronomy and Astrophysics, University of Amsterdam, 1090 GE Amsterdam, The Netherlands

PAUL A. SCOWEN

NASA GSFC

NATALIA SUDNIK

Nicolaus Copernicus Astronomical Centre of the Polish Academy of Sciences, Bartycka 18, 00-716 Warsaw, Poland

STAN P. OWOCKI

Department of Physics and Astronomy, University of Delaware, 217 Sharp Lab, Newark, DE, USA

JON O. SUNDQVIST

Institute of Astronomy, KU Leuven, Celestijnenlaan 200D/2401, 3001 Leuven, Belgium

FLORIAN A. DRIESSEN

Institute of Astronomy, KU Leuven, Celestijnenlaan 200D/2401, 3001 Leuven, Belgium

LEVIN HENNICKER

Institute of Astronomy, KU Leuven, Celestijnenlaan 200D/2401, 3001 Leuven, Belgium

ABSTRACT

The most massive stars are thought to lose a significant fraction of their mass in a steady wind during the main-sequence and blue supergiant phases. This in turn sets the stage for their further evolution and eventual supernova, with consequences for ISM energization and chemical enrichment. Understanding these processes requires accurate observational constraints on the mass-loss rates of the most luminous stars, which can also be used to test theories of stellar wind generation. In the past, mass-loss rates have been characterized via collisional emission processes such as $H\alpha$ and free-free radio emission, but these so-called “density squared” diagnostics require correction in the presence of widespread clumping. Recent observational and theoretical evidence points to the likelihood of a ubiquitously high level of such clumping in hot-star winds, but quantifying its effects requires a deeper understanding of the complex dynamics of radiatively driven winds. Furthermore, large-scale structures arising from surface anisotropies and propagating throughout the wind can further complicate the picture by introducing further density enhancements, affecting mass-loss diagnostics. Time series spectroscopy of UV resonance lines with high resolution and high signal-to-noise are required to better understand this complex dynamics, and help correct “density squared” diagnostics of mass-loss rates. The proposed *Polstar* mission easily provides the necessary resolution at the sound-speed scale of 20 km s^{-1} , on three dozen bright targets with signal-to noise an order of magnitude above that of the celebrated IUE MEGA campaign, via continuous observations that track structures advecting through the wind in real time.

1. INTRODUCTION

Theoretical models of the UV line-driven winds of hot stars (Owocki et al. 1988) predict that internal instabilities should produce high-density clumps and low-density voids, as the hypersonic acceleration cannot be maintained smoothly. Also, in CAK theory (Castor, Abbott, & Klein 1975), the acceleration of the wind depends nonlinearly on the mass flux, so variations in the mass flux launched from the stellar photosphere also produce significant velocity and density variations as the wind

accelerates. Both of these types of wind perturbations will steepen into shocks, compressing and driving dense clumps (Sundqvist et al. 2018), and producing observable hard X-ray emission (e.g., Oskinova 2016 and references therein).

Direct observational evidence that this is occurring even in single stars already exists in optical emission lines of dense winds, in moving emission bumps (e.g., Moffat et al. 1988; Lépine & Moffat 1999) and reduced levels of free-electron scattering in the line wings (Hillier

1991; Hamann & Koesterke 1998). For all these reasons, the concept of a constant mass-flux, smoothly accelerating hypersonic flow is likely not realized in actual winds.

Nevertheless, most current empirical analyses of stellar atmospheres and winds rely on the use of spherical non-LTE model atmospheres. In state-of-art analyses the stellar and wind parameters, such as \dot{M} , are derived by fitting resonance and recombination lines simultaneously. P Cygni lines (often high opacity lines such as C IV) are predominately used to determine terminal wind velocities v_∞ (E.g. Prinja et al. 1990), whereas \dot{M} in the stronger winds of O-stars (mass-loss rates above $10^{-7} M_\odot \text{yr}^{-1}$ (e.g. Mokiem et al. 2007)) is often inferred using H α emission. The latter benefits from arising from what is incontrovertibly the dominant wind species in hot main-sequence stars, ionized H (e.g. Puls et al. 1996).

Yet there is a notable difference between UV resonance lines and (optical) recombination lines such as H α (see left-hand side vs right-hand side of Fig. 2). The resonance lines involve scattering of pre-existing UV stellar continuum, and their optical depth $\propto \rho$, while recombination involves photon creation by collision of 2 particles, such that line emissivities $\propto \rho^2$. The latter also holds for the free-free radio continuum, so crucial indicators of global wind mass-loss rates are sensitive to the local density variations induced by clumping. Thus, use of these “density squared” diagnostics allow inhomogeneities to mimic a higher mass-loss rate. Wind inhomogeneities can also induce strong variations in the local velocity gradients (an effect termed “vorosity” in Sundqvist et al. 2014), which allow more of the stellar continuum to penetrate through the wind opacity of otherwise saturated UV resonance lines, which can mimic a *lower* mass-loss rate in absorption-line diagnostics. Hence, the dual analysis of UV plus optical lines is affected by clumping in subtle and important ways that must be informed by new types of observations.

This has significance not only for our understanding of the wind dynamics themselves, but also for establishing the evolutionary consequences of mass loss during phases of continuous wind outflow, especially the main sequence. The latter is the longest-lived phase of stellar evolution, and happens first, establishing the initial conditions for all subsequent evolutionary phases— including the ultimate supernova of the massive star. Furthermore, the high-mass end of the main sequence has the most profound impact on galactic evolution because it reprocesses the stellar material on such short timescales, all while lower-mass stars are still in their formative stages. Thus, to understand the evolution of massive stars and their impact on the host galaxy in population synthesis studies, we must first accurately determine the mass lost in these decisive initial phases (Langer 2012),

and track how it evolves in the blue supergiant phase. This is especially true for the highest-mass stars, whose wind mass-loss rates are highest and have the greatest evolutionary significance for all subsequent phases of the star, but such stars are also the rarest. Somewhat less massive stars afford more numerous examples to study, and the lessons learned from them place our understanding into a fuller context, so we wish to see the impact of clumping over the fullest possible range of massive stars.

Yet despite the this need for clumping corrections to observationally inferred mass-loss rates, no systematic ultra-high SNR study of clumping and CIR-type features in dynamical spectra of massive star winds has yet been undertaken. The IUE MEGA campaign (Massa et al. 1995) was only able to obtain SNR 20-25, and only on a few targets. The efforts by HST were also limited to a few targets, and were hampered in some cases by pointing difficulties, and an orbit that only allowed continuous observation for about an hour at a time. Hence these past experiments were only able to hint at the presence of clumping and dynamics on scales smaller than the gross “discrete absorption component” (DAC) structures that are often seen in massive-star winds (Kaper et al. 1997), yet these structures are believed to be responsible for extreme density variations necessary to account for the filling-in of P V absorption (Fullerton et al. 2006) and the absence of free-electron scattering wings in dense winds (Hillier 1991).

Enter *Polstar*, whose orbit allows continuous coverage for days, at wavelength resolution $R = 33,000$ in Ch1. One objective (termed *S2*) of the *Polstar* mission is deep, continuous exposures of the 40 brightest massive stars over a range of masses and OB spectral types, to watch clumping and other structure develop in real time in their winds. The fundamental physics of the wind driving is informed by the nature of this clumping, and larger structures such as co-rotating interactions regions (CIRs, c.f. Cranmer & Owocki 1996), as well as prolate/oblate asphericities. But the primary goal of *S2* is to make the necessary corrections to clumping-sensitive mass-loss rate determinations, such as free-free radio (Lamers & Leitherer 1993) and H alpha emission (Puls et al. 1996), because of its importance to stellar evolution as described next.

2. THE IMPORTANCE OF ACCURATE MASS-LOSS RATE DETERMINATIONS

Models of the most massive stars confirm the observational implication that mass loss can play a crucial role in stellar evolution, and accurate knowledge of the mass-loss rate is required for understanding the impact on the host galaxy. Figure 1 presents the evolution of $60 M_\odot$ models computed until the end of central carbon burning, and shows how this evolution is altered when

the mass-loss rates (chosen from Vink et al. 2001) are reduced by a factor of 2 or 3 (here the factors have been applied only during the main sequence, MS). The difference is mainly due to larger winds during the MS (in the standard case) reducing the size of the core, and hence reducing the overall luminosity: at the middle of the MS, the $\dot{M}/2$ model has a core that is 3% larger than the standard model, and the $\dot{M}/3$ has a core that is 5% larger. In the middle of central helium burning, the difference increases, amounting to 50% and 45% respectively. At the end of central C-burning, the CO-core mass (M_{CO}) is 57% (35%) larger in the $\dot{M}/2$ ($\dot{M}/3$) models respectively, leading to very different endpoint locations. A direct effect of changing the mass-loss rates

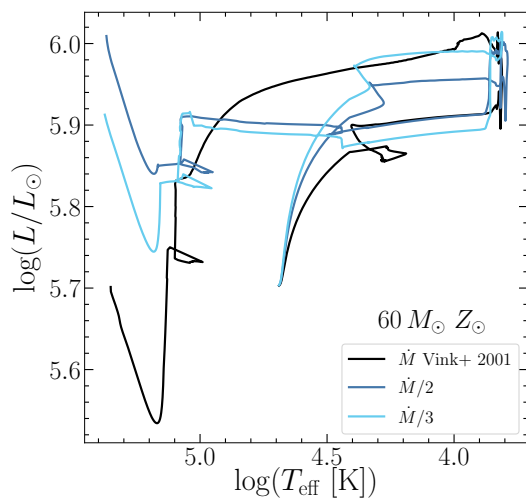


Figure 1. Hertzsprung-Russell diagram of $60 M_{\odot}$ models computed with mass-loss recipe of Vink et al. (2001, black), and the same recipe divided by a factor of 2 and 3 during the MS (teal blue and cyan, respectively).

is the duration of the Wolf-Rayet (WR) phase expected for the models. The standard model becomes a WR early in the He-burning phase ($X(^4\text{He}) = 0.97$), while the lower \dot{M} -rates models arrive later in this regime ($X(^4\text{He}) = 0.29$ and 0.44 respectively). This affects directly their statistical observability.

Surprisingly, the models show that the behaviour is not simply monotonic with the reduction factor on the mass-loss rates, revealing the sensitivity of the advanced phases to what precedes them. In stars, gravity and fusion interact in complex ways, and changing one parameter in the modeling feeds back on all other aspects. Because of its high luminosity at the end of the MS, the $\dot{M}/3$ model loses more mass during the crossing of the Hertzsprung-Russell diagram, spends less time with a $\log(T_{\text{eff}}) < 4.0$, and ends its evolution in an intermediate situation between the standard and the $\dot{M}/2$ models. Hence, changes to mass-loss rates at the factor 2 level can profoundly alter the initial conditions for all

subsequent evolution, ultimately changing the final state where supernova occurs. Since internal structure at all scales can induce such changes in the mass-loss rates inferred from H α and radio emissions, understanding high-mass stellar evolution requires resolving and analyzing the dynamical nature of wind clumping.

3. THE *POLSTAR* EXPERIMENT FOR OBJECTIVE *S2*

The effective area ($A = 50 \text{ cm}^2$ at 150 nm) and spectral resolution ($R = 33,000$) of channel 1 (hereafter Ch1) of the *Polstar* instrument are ideally suited for continuous observing of bright targets that can track features accelerating through the line profile in real time. The spectral resolution ($\cong 10 \text{ km s}^{-1}$) penetrates to the Sobolev scale of thermal Doppler shifts in the metal-ion UV resonance lines observed, and the area A provides sufficient signal-to-noise (SNR) for exposures of duration

$$t = \frac{c}{aR}, \quad (1)$$

where a is the characteristic acceleration rate of the features. The correct value of a is currently unknown, and may vary from star to star, but we might expect it to be of order the stellar surface gravity g , which is typically $\sim 0.03 \text{ km s}^{-2}$. So we will synchronize the exposure time with the rate that features move across resolution elements, and taking a canonical acceleration of $a \sim 0.03 \text{ km s}^{-2}$ implies $t \cong 400\text{s}$. Given *Polstar's* effective area, $t \cong 400\text{s}$ and $R \cong 30,000$ implies the SNR is

$$\frac{S}{N} \cong 90\sqrt{f}, \quad (2)$$

where f is the target flux in units of $10^{-9} \text{ erg cm}^{-2} \text{ s}^{-1} \text{ nm}^{-1}$, a characteristic flux for an average *Polstar* target but somewhat dim for this experiment. Thus dynamical spectra can be produced by continuous monitoring for days, as was done with the IUE MEGA campaign (Massa & Prinja 2015), with greatly improved SNR ($S/N > 400$) for bright targets ($f > 20$).

There are 44 potential targets in our list that satisfy this brightness limit (shown in Table 1). Because of their special importance, we added 2 additional sources (ζ Oph and ϕ Per) that are within a factor of 2 of the brightness limit, for a total of 46 potential targets for the *S2* objective. The mission would select ~ 40 of these for continuous observation over a day or so, based on flexible criteria such as accessibility in the scheduling and overlap with other objectives.

For example, 15 of the targets with $f > 25$ will be prioritized because they also appear in the target list for objective *S3*, relating to rapid rotation causes (Jones et al. 2021), which we can connect with clumping effects. The star ζ Oph was observed by HST for under 5 hours,

but it provides a useful comparison with previous results, and ϕ Per is a variable system involving spinup by binary interaction, allowing the effects of rapid rotation on wind dynamics to be studied. Both added stars will produce $\text{SNR} > 250$, or an order of magnitude above the IUE MEGA campaign, while all the rest exceed $\text{SNR} \cong 400$. This sensitivity is deemed necessary to penetrate the full range of the dynamical structures down to the Sobolev scale $\cong R/100$, since at that scale, we expect $\cong 100^2$ cross sections of Sobolev size across the face of the star, with a statistical variance of some 1 %, requiring SNR at the several-hundred level to confidently resolve.

Once the features are detected, the exposure time ($\cong 400$ s) is matched to the velocity resolution ($\cong 10$ km s^{-1}) to allow the features to be tracked as they accelerate through the wind, to reveal how they initiate and evolve, and quantify their impact on clumping-sensitive mass-loss determinations. And if the acceleration of the features should prove faster than the canonically chosen $a \sim 0.03$ km s^{-2} , even higher SNR will be achieved by simply binning in wavelength. If the features cannot then be resolved at the Sobolev scale (~ 10 km s^{-1}), they can still be resolved at the sonic scale (~ 20 km s^{-1}).

The number of targets in the current plan, ~ 40 , can be monitored for a day or so, or longer in special cases (such as stars like ζ Pup with rotation periods fast enough to study periodicity), within the observing time set aside for this objective (*S2*), as part of the 3-year science mission. This is an opportune number of targets, because it is sufficient to consider trends with mass and spectral type, and it also explores the ubiquity of DACs, and smaller-scale clumps, stemming from either surface perturbations or the LDI.

The other objectives can also benefit from this wealth of observational data on the three dozen brightest massive stars in the sky, as the data can be stacked and binned to achieve unprecedented UV polarization precision. For example, for a median star from the list like γ Cas, stacking over 2-hour chunks to allow temporal variations over the observation to be studied, and binning to $R = 30$ to focus on continuum polarization, would allow a SNR of some 1×10^5 per resolution element. Even with the lower effective area of Ch1, that would support a polarization precision of better than 3×10^{-4} , in the same dataset that would already be mined for its dynamical spectroscopic potential. The polarization information would reveal processes that break the spherical symmetry in a globally steady way, while the dynamical spectra reveal evolving process on much smaller spatial and temporal scales within the wind.

The reason polarimetry is automatically obtained, simultaneously with the spectral information, is that *Pol-*

star determines all four Stokes parameters, I , Q , U , and V , in all its observations. Many of the proposed experiments will use the higher effective area of the low-resolution channel 2 (Ch2) when doing sensitive polarimetry, but in this experiment, the continuous monitoring is in the high-resolution Ch1, so the polarimetric information will come from binning down to low resolution and simply accepting the roughly factor 3 loss of effective area in Ch1.

This loss is mitigated by the use of inherently bright targets, so when the $\text{SNR} \cong 500$ -1000 at $R = 33,000$, it will be $\sqrt{1000}$ times better, or $\cong 15,000$ -30,000, at $R = 33$, a sufficient resolution for using the spectral shape to remove foreground polarization from the interstellar medium citePAndersson2021. Separation from background polarization is also assisted by the time-dependent character of the intrinsic polarization from the wind dynamics. Such high SNR is conducive to polarimetric precision at the required 3×10^{-4} target, which is capable of detecting the temporal variations from some 10,000 clumps with individual free-electron scattering optical depths of 0.1. Hence, the *Polstar* mission objective *S2* will combine dynamical spectra and time-dependent linear polarization variations to track clump and CIR features down to the Sobolev scale, as they accelerate through the winds of 40 bright massive stars, to understand how clumping and structure form, and what is their impact on wind mass-loss rate determinations. It can also detect global structures with very small latitudinal differences in optical depth, down below $\cong 0.01$, due to rotation or other temporally persistent aspherical features, as well as rotationally modulated polarization from large-scale azimuthal structures such as CIRs.

4. SMALL-SCALE CLUMPY WIND STRUCTURE

Due to the variability of spectral lines, as well as the presence of linear polarisation, astronomers have known for decades that stellar winds are not stationary but time-dependent, and that this leads to inhomogeneous, clumpy media (see Puls et al. 2008), Motivated by hydrodynamic simulations (e.g., Feldmeier et al. 1997; Sundqvist & Owocki 2013) including the line-deshadowing instability (LDI) (Owocki et al. 1988), extreme density variations are expected to lead to large root-mean-square density ratios, $D = \sqrt{\langle \rho^2 \rangle} / \langle \rho \rangle$, sometimes called a “filling factor” (though it is not necessary, nor physically realistic, to regard the interclump medium as void). For optical depths that depend linearly on density, such as free-electron optical depth, the mean opacity of a clumped medium is the same as that for a smooth wind, whereas opacities that scale with the square of density (such as for recombination lines like $\text{H}\alpha$), the optical depths are enhanced by the clumping

Table 1. *Polstar* Targets for Structured Wind Studies

Target	Name	Flux (1500Å) (10^{-10} erg/s/cm ² /Å)	SNR eq. (2)
HD 122451	β Cen	600	2200
HD 108248	α Cru	600	2200
HD 116058	α Vir	530	2000
HD 11123	β Cru	400	1800
HD 68273	γ Vel	260	1400
HD 66811	ζ Pup	230	1300
HD 37742		200	1200
HD 37742	ζ Ori	200	1200
HD 116658	Spica	200	1200
HD 35468	γ Ori	190	1200
HD 52089	ϵ CMa	180	1200
HD 44743	β CMa	160	1100
HD 36486	δ Ori	150	1100
HD 24912		130	1000
HD 149438		130	1000
HD 5394	γ Cas	100	900
HD 205021	η Cep	100	900
HD 37043	ι Ori	100	900
HD 34085	Rigel	90	800
HD 127972	η Cen	90	800
HD 143018	π Sco	75	700
HD 151890	μ^1 Sco	70	700
HD 143275	δ Sco	70	700
HD 105435	δ Cen	55	600
HD 106490	δ Cru	55	600
HD 87901	Regulus	50	600
HD 120307	ν Cen	40	500
HD 122451		40	500
HD 136298	δ Lup	37	500
HD 157246	γ Ara	35	500
HD 205021	β Cep	35	500
HD 120324	μ Cen	34	500
HD 147165	σ Sco	32	500
HD 11415	ϵ Cas	31	490
HD 52089	ξ CMa	30	490
HD 121743	ϕ Cen	30	490
HD 37202	ζ Tau	30	490
HD 143118	η Lup	30	490
HD 50013	κ CMa	29	480
HD 19356	Algol	27	460
HD 125238	ι Lup	27	460
HD 3360	ζ Cas	27	460
HD 10144		27	460
HD 10516	ϕ Per	15	350
HD 149757	ζ Oph	10	280

factor D .

The presence of large D values due to extensive micro-clumping (clumps on size scales smaller than a continuum mean-free-path, typical of most hot-star winds) yields an enhancement to mass-loss rates derived from diagnostics that scale with the density squared, such as H α emission. That enhancement is a factor of \sqrt{D} , requiring a corresponding correction to older mass-loss rates derived with the assumption of smooth winds (Mokiem et al. 2007). However, determining the correct value of D is difficult, and is the purpose of objective $S2$. The goal is to use the resonance line opacity that is liberally sprinkled throughout the UV, because it covers a wide range from strong to weak lines, allowing access to wind regions both close to and far from the star, and over a range of wind mass-loss rates.

One challenge with metal resonance lines is that the abundances and degree of ionization can be unknowns. In the EUV, the P v $\lambda\lambda 1118, 1128$ line has the advantage in certain O stars of being expected to be the dominant ionization stage, so should in principle provide an accurate estimate of solely the mass-loss rate. However, Fullerton et al. (2006) selected a large sample of O-stars, which also had ρ^2 (from H α /radio) estimates available, and found that treating resonance lines as though they were linear in ρ required extreme clumping factors of up to $D \sim 400$ (e.g. Bouret et al. 2003).

But UV resonance lines are more complicated than that, because the Sobolev optical depth in such lines depends not on density, but on the ratio of density to velocity gradient, $\rho(dv/dr)^{-1}$. Since the local acceleration, and hence dv/dr , also depends on density, the Sobolev optical depth scales much more steeply than linear in density. For example, if we neglect time dependent terms in the force equation (a rough approximation), and also neglect any feedback between density and line opacities (also imperfect), then at given velocity v and radius r , the standard treatment using the CAK α parameter gives

$$\frac{dv}{dr} \propto \rho^\alpha \left(\frac{dv}{dr} \right)^{-\alpha}. \quad (3)$$

With $\alpha \cong 2/3$, we then have $dv/dr \cong \rho^{-2}$, which implies the Sobolev optical depth in the UV resonance line in question obeys $\tau \propto \rho(dv/r)^{-1} \propto \rho^3$. This is quite a steep dependence, owing to the dependence on velocity gradient, wherein spatial regions of low density yield open holes in velocity space where there is low line optical depth, an effect termed ‘‘vorosity’’ (Sundqvist et al. 2018) in analogy with the ‘‘porosity’’ concept for spatial holes in continuum opacity. Hence clumping alters the degree of absorption in a P Cygni trough, because the vorosity allows a window through the normally optically thick line (Sundqvist et al. 2018), to a degree that we

wish to observe and understand in order to understand the necessary clumping corrections.

4.1. *Optically thick clumping (“macro”-clumping)*

Some analysis of optically thick clumping effects in resonance lines has already been undertaken, taking into account more than just the “filling factor” D , but also the distribution, size, and clump geometry. The conventional description of macro-clumping is based on a clump size, l , and an average spacing of a statistical clump distribution, L , with porosity length $h = L^3/l^2$ (Owocki & Sundqvist 2018). This porosity length h represents the key parameter defining a clumped medium, as it corresponds to the photon mean free path in a medium consisting of optically thick clumps.

Oskinova et al. (2007) employed an “effective opacity” concept in the formal integral for the line profile modelling of the famous O supergiant ζ Pup. Figure 2 shows that the most pronounced effect involves strong resonance lines, such as the resonance doublet P v $\lambda\lambda$ 1118, 1128 which can be reproduced by this macro-clumping approach – without the need for extremely low \dot{M} – resulting from an effective opacity reduction when clumps become optically thick.

Given that H α remains optically thin for O-type stars it is not affected by porosity and it can be reproduced simultaneously with P v $\lambda\lambda$ 1118, 1128. This enabled a solution to the P v $\lambda\lambda$ 1118, 1128 problem (see e.g. Šurlan et al. 2013; Sundqvist & Puls 2018).

4.2. *The origin of wind clumping*

In the canonical view of structure formation via the LDI, clumping would be expected to develop when velocities are sufficiently large to produce shocked structures. For typical O-star winds, this occurs at half the terminal wind velocity, corresponding to roughly 1.5 stellar radii.

Various observational indications, including the existence of linear polarisation (e.g. Davies et al. 2005) and radial dependent Stokes I diagnostics (Puls et al. 2006) indicate that clumping already exists at very low velocities, and likely arises inside the stellar photosphere. Cantiello et al. (2009) suggested that waves produced by the subsurface convection zone could lead to velocity fluctuations, and possibly density fluctuations, and could thus be the root cause for the wind clumping seen close to the stellar surface.

Assuming the horizontal extent of the clumps to be comparable to the vertical extent in terms of the sub-photospheric pressure scale height H_p , one may estimate the number of convective cells by dividing the stellar surface area by the surface area of a convective cell finding that it scales as $(R/H_p)^2$. For main-sequence O stars in the canonical mass range 20-60 M_\odot , pressure scale heights are within the range 0.04-0.24 R_\odot , corre-

sponding to total clump numbers of $6 \times 10^3 - 6 \times 10^4$. These estimates could be tested through linear polarisation monitoring, probing wind clumping close to the wind base.

In an investigation of linear polarisation variability in WR stars, Robert et al. (1989) revealed an anti-correlation between the terminal velocity and the observed scatter in linear polarisation. They interpreted this in terms of blobs growing or surviving more effectively in slower rather than faster winds. Davies et al. (2005) found this trend to continue into the lower temperature regime of the LBVs, whose winds are even slower. Therefore, LBVs are ideal test-beds for constraining wind clump properties – due to their very long wind-flow times. As Davies et al. (2005) found the polarisation angles of LBVs to vary irregularly with time, and optical line polarisation effects were attributed to wind inhomogeneity. Given the short timescale of the observed polarisation variability, Davies et al. (2007) argued that LBV winds consist of order thousands of clumps near the surface. For main-sequence O stars the derivation of the numbers of wind clumps and their sizes from polarimetry has not yet been feasible as very high S/N data is needed. This becomes feasible with the proposed *Polstar* mission, which can reach polarization precision at the 1×10^{-4} level due to very high SNR when the data is binned to $R \cong 30$, as mentioned above.

5. LARGE-SCALE STRUCTURES

5.1. *Magnetically confined winds*

As an additional complication, magnetic fields can influence these hot-star winds significantly, often leading to large-scale structures. Typically, their overall influence on the wind dynamics can be characterized by a single magnetic confinement parameter,

$$\eta_* \equiv \frac{B_{eq}^2 R_*^2}{\dot{M} v_\infty} \quad (4)$$

which characterizes the ratio between magnetic field energy density and kinetic energy density of the wind, as defined in ud-Doula & Owocki (2002). The effects at large η_* are primarily the topic of another *Polstar* white paper (Shultz et al. 2021), but since such magnetic influences are also relevant to clumping and wind asymmetry that affects mass-loss rate diagnostics, and can appear even at low values of η_* , we include a short description here.

Extensive magnetohydrodynamic (MHD) simulations show that, in general, for the stellar models with weak magnetic confinement, $\eta_* < 1$ field lines are stretched into radial configuration by strong outflow very quickly on a dynamical timescale. However, even for magnetic confinement as weak as $\eta_* \sim 1/10$ the field can have enough influence to enhance density by diverting the

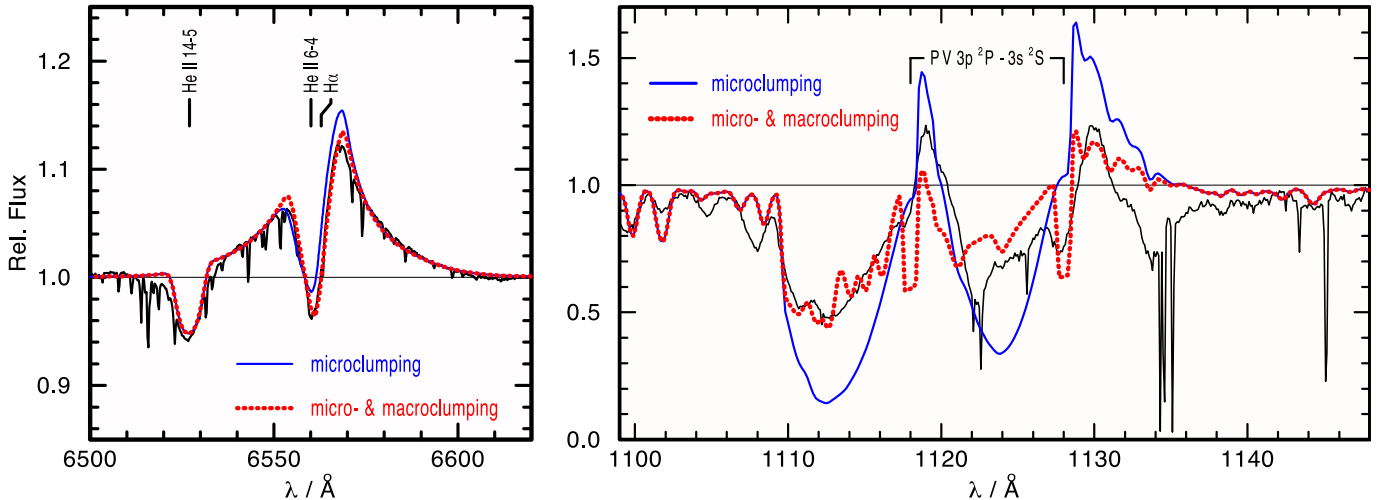


Figure 2. Porosity as the likely solution for the PV problem. The $H\alpha$ line on the left-hand side is hardly affected by macroclumping, while the $P\ V\ \lambda\lambda 1118, 1128$ UV line on the right is strongly affected. Adapted from [Oskinova et al. \(2007\)](#).

wind material from higher latitudes towards the magnetic equator.

On the other hand, for stronger confinement, $\eta_* > 1$, the magnetic field remains closed over a limited range of latitude and height about the equatorial surface, but eventually is opened into a nearly radial configuration at large radii. Within closed loops, the flow is channeled toward loop tops into shock collisions where the material cools and becomes dense. With the stagnated material then pulled by gravity back onto the star in quite complex and variable inflow patterns. Within open field flow, the equatorial channeling leads to oblique shocks that eventually lead to a thin, dense, slowly outflowing “disk” at the magnetic equator. This is in concert with the “magnetically confined wind shock” model first forwarded by [Babel & Montmerle \(1997\)](#). Such large scale wind structures are inferred most directly from time variability in the blueshifted absorption troughs of UV P Cygni profiles.

More recent MHD modelling shows that the wind structure and wind clumping properties change strongly with increasing wind-magnetic confinement. In particular, in strongly magnetically confined flows, the LDI leads to large-scale, shellular sheets (‘pancakes’) that are quite distinct from the spatially separate, small-scale clumps in non-magnetic hot-star winds ([Driessen et al. 2021](#)).

5.2. Discrete Absorption Components

Early high-resolution ultraviolet spectroscopy of massive stars obtained with the Copernicus satellite revealed the presence of sharp absorption features superimposed onto the extended blueshifted absorption troughs of far ultraviolet (FUV) resonance lines ([Underhill 1975](#); [Morton 1976](#); [Snow & Morton 1976](#)), often located near the

terminal wind velocity. Initially dubbed “narrow absorption components”, or NACs, they were later found to be snapshots of a dynamic feature now known as “discrete absorption components” (or DACs). The discovery of DACs was made possible by the advent of time-resolved high-resolution FUV spectroscopic observations obtained with the International Ultraviolet Explorer (IUE). They were found to start out as broad, shallow absorption features at low velocity, narrowing and deepening (in some cases saturating) as they migrate to higher velocities over characteristic timescales on the order of days (e.g. [Prinja et al. 1987](#)). Furthermore, they were found to occur nearly ubiquitously among O stars ([Howarth & Prinja 1989](#)). Since they cover a large range of velocities in the absorption trough, they must be caused by features covering a large radial extent within the stellar wind, and be indicative of a physical process universally present in massive stars.

Determining whether the variability seen in the UV time series spectra is due to material originating near or at the surface of the star and then propagating outward, or low speed material at large distances from the star which simply appears at low velocity is a goal that we seek to address with *Polstar*. Should the origin of all of the features be tied to the stellar surface, this would have implications about the structure of the winds (how does the component of the wind which shapes saturated wind lines co-exist with large scale structure), the structure of the photosphere (what are causes the photospheric irregularities that give rise to the different wind flows), X-ray production (can some X-rays originate along the interfaces of the CIRs) and the theoretical derivations and simulations based on a smooth wind.

Generally, there is no way to directly determine the location in the wind where an absorption feature at a

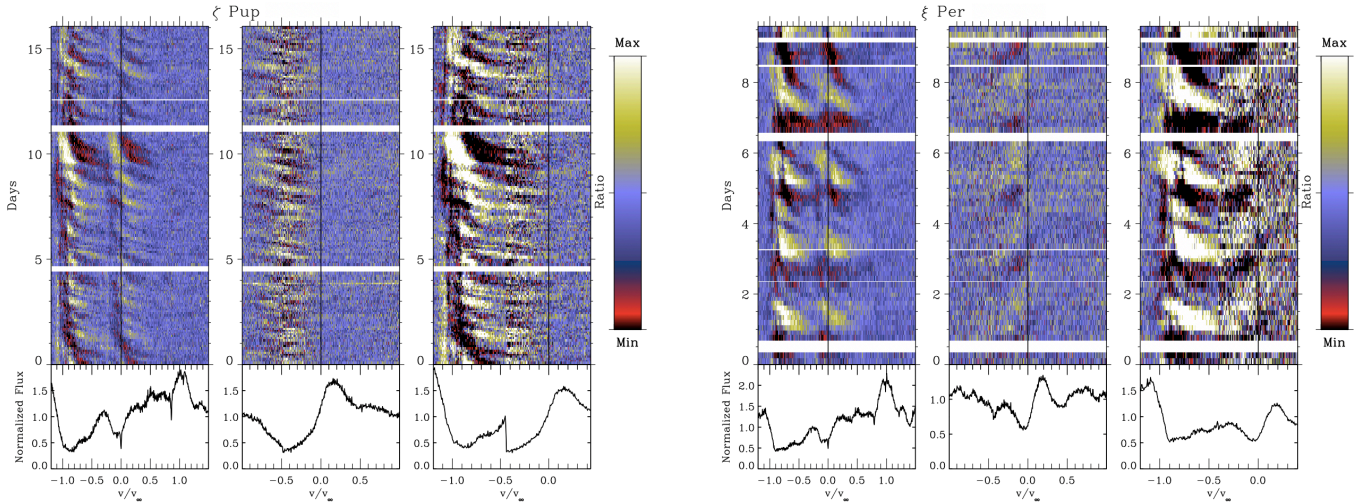


Figure 3. Dynamical spectra as deviations from the mean profiles shown at bottom, taken from the IUE MEGA project for ζ Pup and ξ Per. Strong (left) and weak (center) lines are spliced together (right) to show the continuous acceleration of the DAC features (Massa & Prinja 2015).

specific velocity originates. For example, a low velocity feature could be near the stellar surface, accelerating outward, or due to a slowly moving parcel of wind material far out in the wind, which is re-accelerating after being shocked. This ambiguity is always the case for resonance lines, but not for excited state lines. An excited state wind line arises from an allowed transition whose lower level is the upper level of a resonance transition (typically below 900Å). They frequently appear as wind lines in O stars with strong mass fluxes. One of the most commonly observed excited state lines is N IV λ 1718Å, whose lower level is the upper level of the N IV λ 765Å resonance line. Because a strong EUV radiation field is required to populate an excited state line, these lines can only exist close to the star (this is what gives excited state lines their distinctive shapes). As a result, a feature which appears at low velocity in an excited state line must originate close to the stellar surface

Unfortunately, this same property means that excited state lines weaken quickly at large distances from the star and, as a result, rarely extend to very high velocities. This challenge can be met however by the superior S/N spectra offered by *Polstar*. We see, therefore, how resonance and excited state lines complement one another. If a feature (indicated by excess or reduced absorption) appears at low velocity in an excited state line and then joins a high velocity feature in a resonance line (whose low velocity portion may be saturated), this provides evidence that the excess or deficiency of absorbing material which caused the feature originated close to the stellar surface (where the radiation field is intense) and then propagated outward, into the wind.

A powerful diagnostic is to compare and ‘splice’ to-

gether the temporal behaviour seen in the Si IV λ 1400Å resonance line doublet and N IV λ 1718Å excited state singlet (cite ζ Pup and ξ Per figures). Our analysis is relatively simple, and based primarily on inspection of dynamic spectra. Dynamic spectra are images of time ordered spectra normalized by the mean spectrum of the series. The properties of coherent structure seen in the full comparison between these lines will allow us to (i) test whether every absorption feature observed at low/near-zero velocity connects to a feature at high velocity. (ii) reveal “banana” shaped patterns, which are the accepted signatures of CIRs tied to the stellar surface. (iii) establish connections between the wind features and the stellar surface. (iv) constrain any instances of evidence features formed (at intermediate velocity) in the wind: if all features can be traced back to the surface and they move through the profile monotonically with velocity, this would imply that we only see evidence for porosity in the dynamic spectra, and not “vorocity”. (v) test the notion that features in dynamic spectra must be huge, with large lateral extent in order to remain in the line of sight for days, persisting to very large velocity.

5.3. Corotating Interaction Regions

As mentioned above, one of the leading hypotheses to explain DACs involves large-scale structures extending through most of the radial extent of the wind. Mullan (1986) suggested that “corotating interaction regions” (or CIRs), as seen in the solar wind, could be responsible for the observed phenomenology. This model involves rotation of the star changing the conditions at the footpoint of flows along the line of sight to the observer, producing regions of either stronger or weaker

wind that interact because of their different accelerations along that line.

One way to achieve this quasi-periodic footpoint modulation is to adopt *ad hoc* brightness spots on the stellar surface. [Cranmer & Owocki \(1996\)](#) tested both dark and bright spots using 2D hydrodynamical simulations, finding that only synthetic line profiles computed using the CIRs that emanate from bright spots reproduce the observed DAC structure. Also, they found that while there was a slight overdensity within the CIRs, the real source of the enhanced absorption in DACs stems from the velocity plateau (or “kink”) that arises when sparser, faster material from the bulk of the wind plows into the denser, slower material driven by the bright spots.

This model did not attempt to account for the existence of spots, although some ideas have been suggested, including the possibility that magnetic flux tubes could be causing depressions in the stellar surface to maintain lateral balance in the combined gas and magnetic pressure. These depressions could penetrate to higher temperatures and produce brightening, and growing observational evidence suggests this may occur in a variety of massive stars not observed to have globally strong fields (e.g., [Balona 2019](#); [Momany et al. 2020](#)). However, weak photometric variations ([Ramiamananantsoa et al. 2018](#)) place problematical constraints on the size and brightness of spots that could seed wind features large enough to explain DACs, so the interpretation remains unclear.

The combination of high spectral resolution with polarimetric sensitivity, such as provided by *Polstar*, can help constrain the attributes of the structures responsible for DACs. The IUE MEGA campaign well characterized DACs in the time domain for only a few targets, and at a SNR that could only detect the largest features. But the full nature of such features remains ambiguous when all that is available is information about their projection against the star, and the interpretation of the line Doppler shifts, though valuable, is complicated by the details of the velocity structure.

The potential for complexity is exhibited in Fig. (4), where shown is the resonance zones in a CIR-type model structure. Dynamical spectra include a wealth of information from the time domain about structure along the path to the stellar disk, but polarization information from the wind patterns as they turn away from that disk complements these constraints. Polarization information from Ch1 is automatically obtained with the *Polstar* dynamical spectra, and binning to low resolution increases the sensitivity dramatically. The foreground polarization from dust in the interstellar medium will be separated from the intrinsic signal using means described in more detail in the *Polstar* white paper focused on the interstellar medium signal ([Andersson et al.](#)

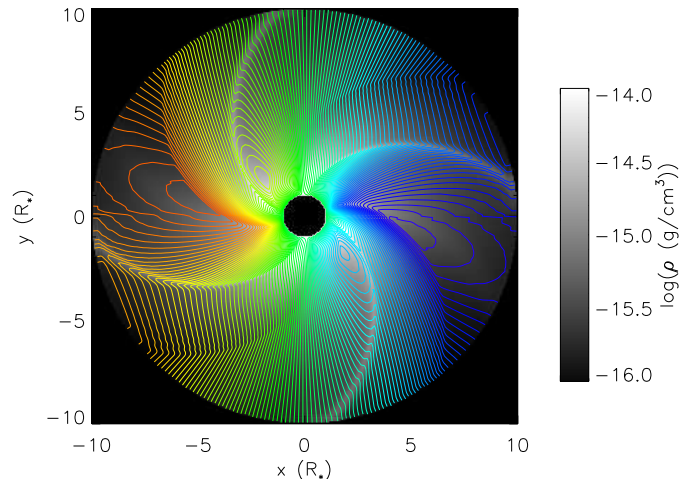


Figure 4. Adapted from [David-Uraz et al. \(2017\)](#): 2D equatorial slice of a wind with CIRs created by four equally spaced bright spots. The greyscale background represents density, and color-coded line-of-sight isovelocity contours are overlaid for an observer along the positive x-axis (blue corresponds to high-velocity blue-shifted material, and red to high-velocity red-shifted material). A 50 km s^{-1} resolution is shown, illustrating that the $\sim 10 \text{ km s}^{-1}$ resolution achievable with *Polstar* will spatially sample the complex structure of the wind material very effectively. This will continue to be true when the data is binned to 20 km s^{-1} resolution to obtain the high SNR desired in this experiment. The figure demonstrates that when large-scale structure is present, spatial resolution cannot be simply interpreted from the Doppler shifts in the line profile; additional geometric information from continuum polarization will be necessary to resolve ambiguities in the global structure.

[2021](#)). This involves wavelength-dependent signatures that only require some 30 points per spectrum, rather than the 30,000 available in the dynamical spectra, so binning by a factor of 1000 will be used to raise the SNR from > 400 in Table (3) to $> 10,000$, suitable for the required 3×10^{-4} polarization sensitivity target, with margin.

The DACs themselves have been well characterized at the IUE SNR, but their impact on the inferred mass-loss rates is only significant if they represent a peak in a hierarchy of smaller structures that IUE did not have the SNR to detect. Also, High spectral resolution can provide good information about the spatial distribution of material in the wind

While DACs repeat in the dynamic spectra of OB stars (e.g. [Kaper et al. 1996](#)), they are not strictly periodic. Nevertheless, they are characterized by a timescale that is understood to be related to the rotation period of a star ([Prinja 1988](#)). This rotational modulation prompted the hypothesis that CIRs might be a consequence of large-scale magnetic fields on the surfaces of massive stars, as have since been detected on a subset of them ([Grunhut et al. 2017](#)) – interacting with the stellar wind to form “magnetospheres”, as discussed

above. However, using high-quality optical spectropolarimetric data, [David-Uraz et al. \(2014\)](#) have placed stringent upper limits on the magnetic field strengths of a sample of 13 well-studied OB stars with extensive FUV time-resolved spectra. They conclusively demonstrated that large-scale fields could not exert sufficient dynamic influence on the wind to form CIRs. An alternative explanation involves non-radial pulsations (NRPs), but reconciling their typical periods with the DAC recurrence timescales requires complex mode superpositions ([de Jong et al. 1999](#)). Therefore, the prevailing hypothesis regarding the origin of putative CIRs involves the presence of spots on the stellar surface.

5.4. Surface spots

Even if surface spots seem a promising cause of CIR structures, the reasons behind their presence remain unclear. Unlike lower-mass Ap/Bp stars and chemically peculiar intermediate mass stars (such as Am stars and HgMn stars), early-type OB stars are not expected to have chemical abundance spots, as they would be continuously stripped by the wind (e.g. [Michaud et al. 1987](#)). One possible mechanism by which such brightness spots can be formed involves small-scale magnetic fields. A possible consequence of convective motions in the subsurface convection zone due to the iron opacity peak (FeCZ; [Cantiello et al. 2009](#); [Schultz et al. 2020](#)), magnetic spots can lead to brightness enhancements by locally reducing the gas pressure, and hence the optical depth. This creates a sort of “well”, allowing us to see hotter plasma, deeper inside the envelope ([Cantiello & Braithwaite 2011](#)). While such spots have yet to be detected in OB stars, weak structured fields have now been detected on several A-type stars (e.g. [Petit et al. 2017](#)). There have also been further theoretical advances suggesting that stars with radiative envelopes can either have large-scale fields strong enough to inhibit convection in the FeCZ, or weak, disorganized fields generated by that convection ([Jermyn & Cantiello 2020](#)), leading to a bimodal distribution of field strengths and thus explaining the so-called ‘magnetic desert’ ([Aurière et al. 2007](#)).

Regardless of their physical origin (localized magnetic fields or NRPs), bright spots have been detected on at least two archetypal massive stars: ξ Per ([Ramiamanantsoa et al. 2014](#)) and ζ Pup ([Ramiamanantsoa et al. 2018](#)). These initial studies suggest that the spots are large (angular radius greater than $\sim 10^\circ$) and relatively persistent (lasting roughly tens of rotational cycles), and lead to fairly faint variability (about 10 mmag in the optical – only detectable with space-based facilities). Assuming that these are hot spots (which means that their brightness enhancement in the ultraviolet compared to the surrounding photosphere is greater

than in the optical), further hydrodynamical simulations carried out by [David-Uraz et al. \(2017\)](#) showed that the spot properties inferred from the light curve of ξ Per could also lead to CIRs that quantitatively reproduce the DACs observed for this star. Clearly the UV band has much to say about the importance of these spots, and *Polstar*’s observations will have a lot to contribute to this issue, while in the process of establishing corrections to the mass-loss rates.

6. HYDRODYNAMIC MODELING

Recent models of the line-driven instability (LDI) using 2D hydrodynamics driven by 1D radiative transfer, simplified to allow dynamical resolution of the resulting clumping, gives the density structure shown in Fig. (5). These models do not use any variations at the lower boundary, so the extreme degree of clumping is entirely self-excited due to the rapid growth rate of the intrinsic instability. The lateral scale is limited only by the tiny scale ($\cong R/100$) of the Sobolev length, producing thousands of clumps in all. As the radial scale is stretched out by the radial instability in the velocity gradient, the clumps appear radially elongated, which causes them to produce absorption fluctuations that are wide in velocity ($> 100 \text{ km s}^{-1}$), but only a few percent in depth, as can be seen in the time varying P Cygni profile in Fig. (6).

Since the model is only 2D, there is an artificial azimuthal symmetry around the line to the observer, which produces circularly coherent structures that overestimates the magnitude of the variances shown. Assuming the azimuthal coherence length should actually be on the Sobolev scale, $\cong R/100$, an order of magnitude of cancellation in the temporal variations could be expected. This will require further modeling to explore, but given that the largest features have a variance approaching 10% in this azimuthally symmetric treatment, the largest temporal variations might appear at the 1% level or less. Nevertheless, the *Polstar* experiment described above achieves SNR in the range 400 - 1000, depending on the target brightness, so temporal variations over a day-long observation could easily characterize variances at the 1 % level, or even less. The intended binning to 20 km s^{-1} resolution will also easily resolve the model features, which typically show a velocity width $> 100 \text{ km s}^{-1}$.

The dynamical spectrum produced by this model is shown in Fig. (6). Again the artificial azimuthal coherence in the model may overestimate the scale of the features, but their general attributes are seen to be highly reminiscent of observed dynamical spectra. The model features have an acceleration that is seen to be nearly constant, and somewhat faster than what has been so far observed (the scale of the acceleration in the simulation

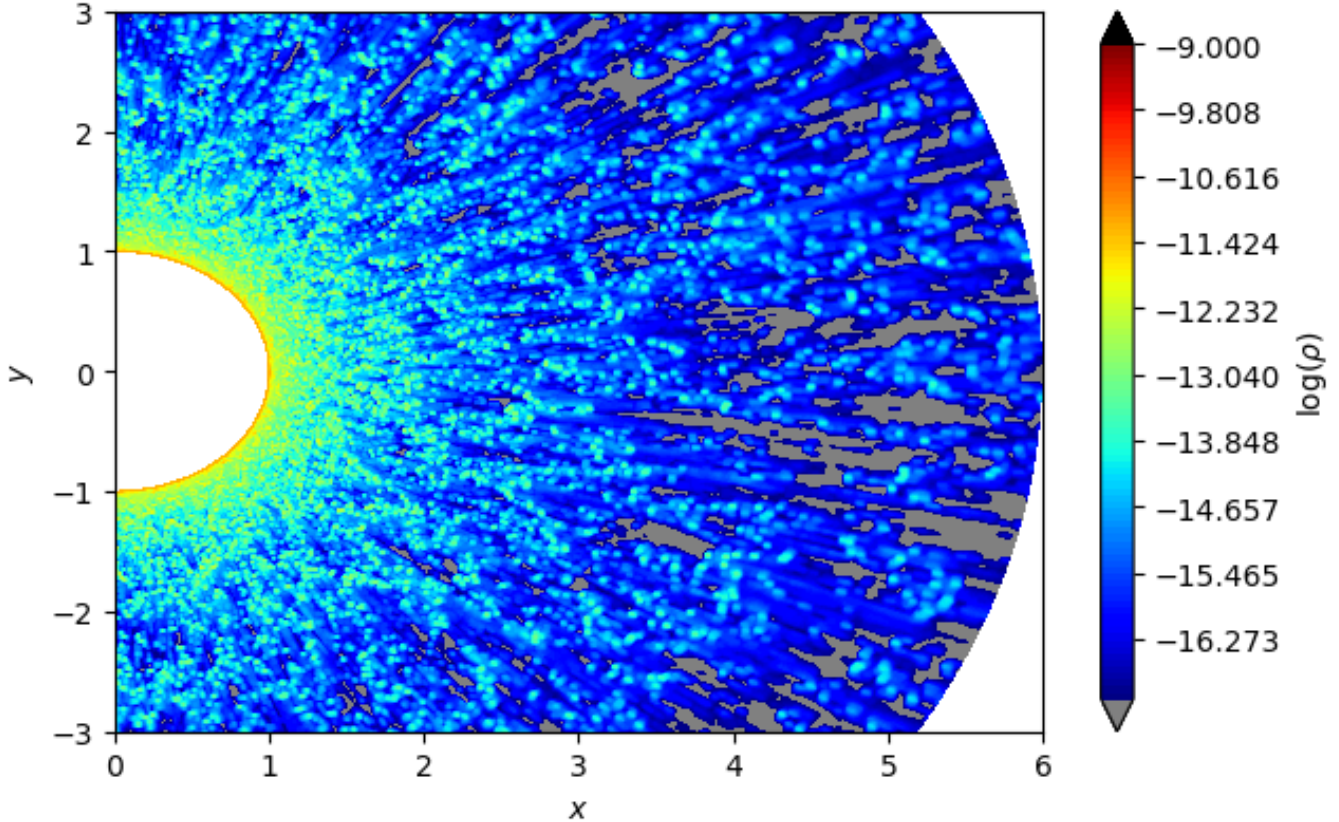


Figure 5. Shown is the density structure in the 2D LDI simulation. To limit computing time, the radiative driving is entirely radial.

is $\cong 0.2 \text{ km s}^{-2}$, whereas the few observed accelerations are perhaps about 1/4 that rapid). This may be because observed features are primarily limited to large DACs that may be linked to CIRs induced by rotating surface features such as spots, not the intrinsic wind features simulated here.

The higher SNR accessible by the *Polstar S2* experiment will allow us to ascertain whether there are different acceleration rates for features linked to surface inhomogeneities, as opposed to self-excited clumps in the wind. If such potentially more rapid accelerations exist in the data, the wide features that appear in the simulation shown can still be temporally tracked using the exposure times in this experiment by binning the data to 100 km s^{-2} , approximately doubling the already high SNR in the process. Alternatively, if the accelerations are more at the scale of the surface gravity of the star, as may tend to be true of the few DACs that have been well resolved, then the finer binning at the sound speed level ($\cong 20 \text{ km s}^{-1}$) will match well the exposure times and produce the experiment described in section 3 above.

Also, the seeming quasi-periodicity seen in these simulations, despite including no rotation, allows for the possibility that the wind is “flapping” on its own intrinsic timescale. These day-long timescales might then

be only coincidentally related to rotation periods of fast rotators like zeta Puppis, and the DACs might then be unrelated to spots or CIR features. This possibility can also be tested by the *Polstar S2* experiment, because enough stars will be targeted to include a range of inclinations and rotation rates. CIR-type structures would depend on those variables, but not intrinsic wind effects.

It should be noted that although these simulations include the LDI, they also involved physically motivated boundary conditions that are conducive to surface variations from the “nodal topology” of the line-driven critical point citep2015MNRAS.453.3428S. Hence, it is not yet clear if the features seen in these simulations develop in the wind due to the instability, or propagate from the surface due to the nonlinearity of the driving.

Finally, the fact that observed DACs must cover a significant fraction of the stellar disk (in order to produce such deep features) presents challenges to every one of these models. With an order of magnitude improvement in SNR over the IUE MEGA campaign, *Polstar* will be able to search for a hierarchy of smaller structures that cover less of the stellar disk, to place the more blatant DAC structures into a fuller context of other features that will help ascertain their true nature.

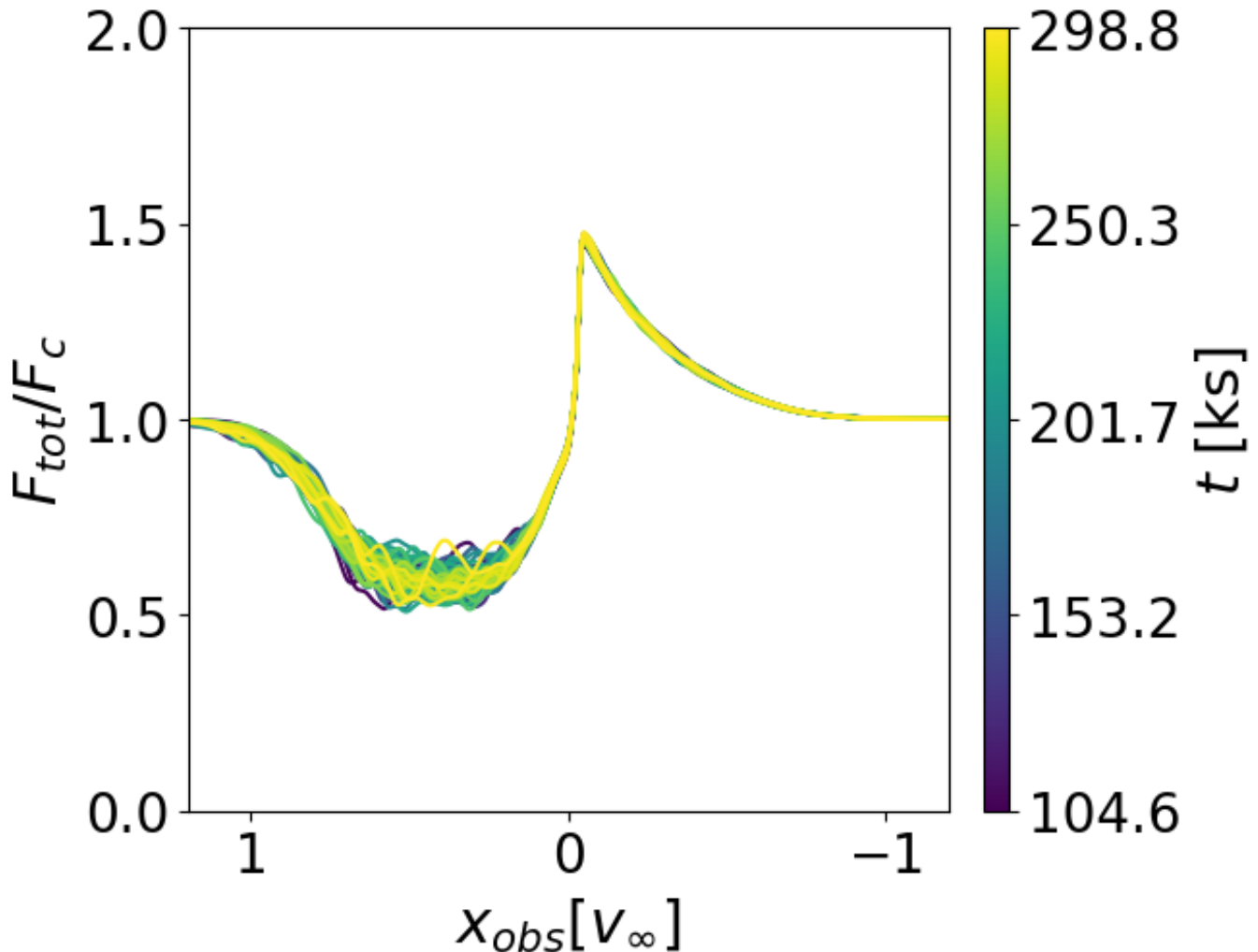


Figure 6. Temporal snapshots of the P Cygni profile variations from the LDI simulation, showing variations of width $> 100 \text{ km s}^{-1}$. The depth of the features is enhanced artificially in the 2D model by azimuthal coherence around the observer line of sight, and could be an order of magnitude less. The mean shape of the P Cygni absorption is less deep than a smooth model, owing to the effects of “vorosity”.

7. EVIDENCE FOR STRUCTURE FROM POLARIZATION

As described above, the *Polstar* mission will include polarization measurements in support of objective *S2* taken in Ch1 and binned in wavelength to increase the SNR to the levels required to detect small polarization signals at the level of a few times 10^{-4} . The goal will be to detect free electron scattering in large-scale wind structures like CIRs, and also time variation in the polarization position angle due to stochastic scattering in a host of smaller scale clumps. Also, if surface spots play a role in inducing the wind structure, especially the large-scale DAC structures, the location on the stellar surface of these spots, when near the limb, can be correlated with the position angle they produce. This is the manner in which polarization information complements the spectroscopic signals, but for targets with a significant

polarization contribution from the interstellar medium (ISM), the ISM component will need to be removed. This will be done using the well-understood wavelength dependence of the ISM component, as well as its expected time independence, contrasted with the time dependence of the intrinsic stellar component. More details are given in the white paper describing the objectives related to ISM polarization (Andersson et al. 2021), as mentioned previously.

8. CONCLUSIONS

The *Polstar S2* experiment is built to resolve and track small-scale clumping in line-driven winds at SNR > 400 , and also to connect larger scale structure with UV polarization signatures stemming from free-electron scattering. The purpose is to quantify corrections of mass-loss rate determinations that are sensitive to den-

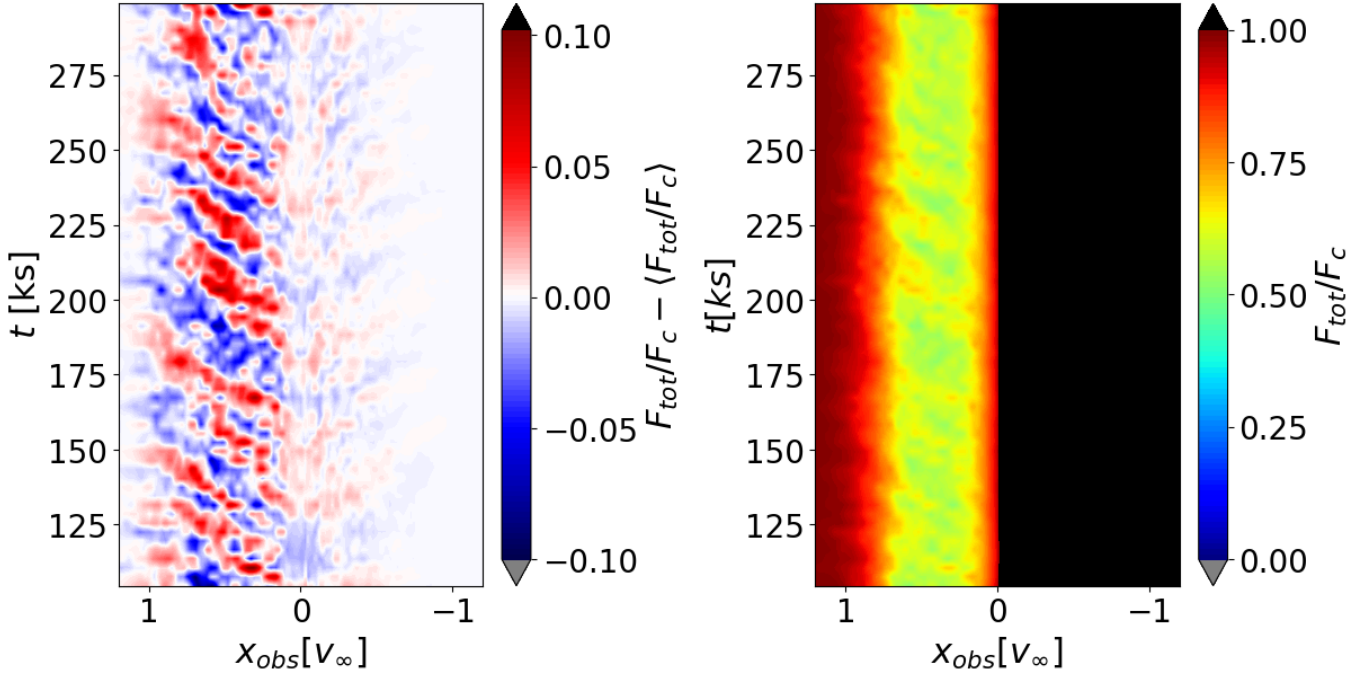


Figure 7. Dynamical spectra from the LDI model are shown relative to the mean profile on the left, and for the full profile on the right. The velocity and temporal widths of the features are true to the simulation, but their magnitude is overestimated by perhaps an order of magnitude because of the model 2D azimuthal symmetry around the observer line of sight.

sity inhomogeneity, such as H α and free-free radio emission. This will lead to more accurate determinations of how much mass high-mass main-sequence stars and blue supergiants lose, setting the stage for, and significantly altering, later evolutionary phases for single stars and binaries alike. In the process, the physics of the driving of these winds, and their profound importance on galactic ecology, will be better understood.

RI acknowledges funding support from a grant by the National Science Foundation, AST-2009412. Scowen acknowledges his financial support by the NASA Goddard Space Flight Center to formulate the mission proposal for *Polstar*. Y.N. acknowledges support from the Fonds National de la Recherche Scientifique (Belgium), the European Space Agency (ESA) and the Belgian Federal Science Policy Office (BELSPO) in the framework of the PRODEX Programme (contracts

linked to XMM-Newton and Gaia). SE acknowledges the STAREX grant from the ERC Horizon 2020 research and innovation programme (grant agreement No. 833925), and the COST Action ChETEC (CA 16117) supported by COST (European Cooperation in Science and Technology). A.D.-U. is supported by NASA under award number 80GSFC21M0002. AuD acknowledges support by NASA through Chandra Award number TMI-22001B issued by the Chandra X-ray Observatory 27 Center, which is operated by the Smithsonian Astrophysical Observatory for and on behalf of NASA under contract NAS8-03060. NS acknowledges support provided by NAWA through grant number PPN/SZN/2020/1/00016/U/DRAFT/00001/U/00001. LH, FAD, and JOS acknowledge support from the Odysseus program of the Belgian Research Foundation Flanders (FWO) under grant G0H9218N.

REFERENCES

- Andersson, B.-G., Clayton, G. C., Doney, K. D., et al. 2021, *Ultraviolet Spectropolarimetry with Polstar: Interstellar Medium Science*. <https://arxiv.org/abs/2111.08079>
- Aurière, M., Wade, G. A., Silvester, J., et al. 2007, *A&A*, 475, 1053, doi: [10.1051/0004-6361:20078189](https://doi.org/10.1051/0004-6361:20078189)
- Babel, J., & Montmerle, T. 1997, *A&A*, 323, 121
- Balona, L. A. 2019, *MNRAS*, 490, 2112, doi: [10.1093/mnras/stz2808](https://doi.org/10.1093/mnras/stz2808)
- Bouret, J. C., Lanz, T., Hillier, D. J., et al. 2003, *ApJ*, 595, 1182, doi: [10.1086/377368](https://doi.org/10.1086/377368)
- Cantiello, M., & Braithwaite, J. 2011, *A&A*, 534, A140, doi: [10.1051/0004-6361/201117512](https://doi.org/10.1051/0004-6361/201117512)
- Cantiello, M., Langer, N., Brott, I., et al. 2009, *A&A*, 499, 279, doi: [10.1051/0004-6361/200911643](https://doi.org/10.1051/0004-6361/200911643)
- Castor, J. I., Abbott, D. C., & Klein, R. I. 1975, *ApJ*, 195, 157, doi: [10.1086/153315](https://doi.org/10.1086/153315)
- Cranmer, S. R., & Owocki, S. P. 1996, *ApJ*, 462, 469, doi: [10.1086/177166](https://doi.org/10.1086/177166)

- David-Uraz, A., Owocki, S. P., Wade, G. A., Sundqvist, J. O., & Kee, N. D. 2017, *MNRAS*, 470, 3672, doi: [10.1093/mnras/stx1478](https://doi.org/10.1093/mnras/stx1478)
- David-Uraz, A., Wade, G. A., Petit, V., et al. 2014, *MNRAS*, 444, 429, doi: [10.1093/mnras/stu1458](https://doi.org/10.1093/mnras/stu1458)
- Davies, B., Oudmaijer, R. D., & Vink, J. S. 2005, *A&A*, 439, 1107, doi: [10.1051/0004-6361:20052781](https://doi.org/10.1051/0004-6361:20052781)
- de Jong, J. A., Henrichs, H. F., Schrijvers, C., et al. 1999, *A&A*, 345, 172
- Diessen, F. A., Kee, N. D., & Sundqvist, J. O. 2021, arXiv e-prints, arXiv:2110.05302, <https://arxiv.org/abs/2110.05302>
- Feldmeier, A., Puls, J., & Pauldrach, A. W. A. 1997, *A&A*, 322, 878
- Fullerton, A. W., Massa, D. L., & Prinja, R. K. 2006, *ApJ*, 637, 1025, doi: [10.1086/498560](https://doi.org/10.1086/498560)
- Grunhut, J. H., Wade, G. A., Neiner, C., et al. 2017, *MNRAS*, 465, 2432, doi: [10.1093/mnras/stw2743](https://doi.org/10.1093/mnras/stw2743)
- Hamann, W. R., & Koesterke, L. 1998, *A&A*, 335, 1003
- Hillier, D. J. 1991, *A&A*, 247, 455
- Howarth, I. D., & Prinja, R. K. 1989, *ApJS*, 69, 527, doi: [10.1086/191321](https://doi.org/10.1086/191321)
- Jermyn, A. S., & Cantiello, M. 2020, *ApJ*, 900, 113, doi: [10.3847/1538-4357/ab9e70](https://doi.org/10.3847/1538-4357/ab9e70)
- Jones, C. E., Labadie-Bartz, J., Nazé, Y., et al. 2021, arXiv e-prints, arXiv:2111.07926, <https://arxiv.org/abs/2111.07926>
- Kaper, L., Henrichs, H. F., Nichols, J. S., et al. 1996, *A&AS*, 116, 257
- Kaper, L., Henrichs, H. F., Fullerton, A. W., et al. 1997, *A&A*, 327, 281
- Lépine, S., & Moffat, A. F. J. 1999, *ApJ*, 514, 909, doi: [10.1086/306958](https://doi.org/10.1086/306958)
- Massa, D., & Prinja, R. K. 2015, *ApJ*, 809, 12, doi: [10.1088/0004-637X/809/1/12](https://doi.org/10.1088/0004-637X/809/1/12)
- Massa, D., Fullerton, A. W., Nichols, J. S., et al. 1995, *ApJL*, 452, L53, doi: [10.1086/309707](https://doi.org/10.1086/309707)
- Michaud, G., Dupuis, J., Fontaine, G., & Montmerle, T. 1987, *ApJ*, 322, 302, doi: [10.1086/165726](https://doi.org/10.1086/165726)
- Moffat, A. F. J., Drissen, L., Lamontagne, R., & Robert, C. 1988, *ApJ*, 334, 1038, doi: [10.1086/166895](https://doi.org/10.1086/166895)
- Mokiem, M. R., de Koter, A., Evans, C. J., et al. 2007, *A&A*, 465, 1003, doi: [10.1051/0004-6361:20066489](https://doi.org/10.1051/0004-6361:20066489)
- Momany, Y., Zaggia, S., Montalto, M., et al. 2020, *Nature Astronomy*, 4, 1092, doi: [10.1038/s41550-020-1113-4](https://doi.org/10.1038/s41550-020-1113-4)
- Morton, D. C. 1976, *ApJ*, 203, 386, doi: [10.1086/154090](https://doi.org/10.1086/154090)
- Mullan, D. J. 1986, *A&A*, 165, 157
- Oskinova, L. M., Hamann, W. R., & Feldmeier, A. 2007, *A&A*, 476, 1331, doi: [10.1051/0004-6361:20066377](https://doi.org/10.1051/0004-6361:20066377)
- Owocki, S. P., Castor, J. I., & Rybicki, G. B. 1988, *ApJ*, 335, 914, doi: [10.1086/166977](https://doi.org/10.1086/166977)
- Owocki, S. P., & Sundqvist, J. O. 2018, *MNRAS*, 475, 814, doi: [10.1093/mnras/stx3225](https://doi.org/10.1093/mnras/stx3225)
- Petit, P., Hébrard, E. M., Böhm, T., Folsom, C. P., & Lignières, F. 2017, *MNRAS*, 472, L30, doi: [10.1093/mnras/1/slx132](https://doi.org/10.1093/mnras/1/slx132)
- Prinja, R. K. 1988, *MNRAS*, 231, 21P, doi: [10.1093/mnras/231.1.21P](https://doi.org/10.1093/mnras/231.1.21P)
- Prinja, R. K., Barlow, M. J., & Howarth, I. D. 1990, *ApJ*, 361, 607, doi: [10.1086/169224](https://doi.org/10.1086/169224)
- Prinja, R. K., Howarth, I. D., & Henrichs, H. F. 1987, *ApJ*, 317, 389, doi: [10.1086/165285](https://doi.org/10.1086/165285)
- Puls, J., Markova, N., Scuderi, S., et al. 2006, *A&A*, 454, 625, doi: [10.1051/0004-6361:20065073](https://doi.org/10.1051/0004-6361:20065073)
- Puls, J., Vink, J. S., & Najarro, F. 2008, *A&A Rv*, 16, 209, doi: [10.1007/s00159-008-0015-8](https://doi.org/10.1007/s00159-008-0015-8)
- Puls, J., Kudritzki, R. P., Herrero, A., et al. 1996, *A&A*, 305, 171
- Ramiaramantsoa, T., Moffat, A. F. J., Chené, A.-N., et al. 2014, *MNRAS*, 441, 910, doi: [10.1093/mnras/stu619](https://doi.org/10.1093/mnras/stu619)
- Ramiaramantsoa, T., Moffat, A. F. J., Harmon, R., et al. 2018, *MNRAS*, 473, 5532, doi: [10.1093/mnras/stx2671](https://doi.org/10.1093/mnras/stx2671)
- Robert, C., Moffat, A. F. J., Bastien, P., Drissen, L., & St.-Louis, N. 1989, *ApJ*, 347, 1034, doi: [10.1086/168194](https://doi.org/10.1086/168194)
- Schultz, W., Bildsten, L., & Jiang, Y.-F. 2020, *ApJ*, 902, 67, doi: [10.3847/1538-4357/abb405](https://doi.org/10.3847/1538-4357/abb405)
- Shultz, M. E., Casini, R., Cheung, M. C. M., et al. 2021, arXiv e-prints, arXiv:2111.06434, <https://arxiv.org/abs/2111.06434>
- Snow, T. P., J., & Morton, D. C. 1976, *ApJS*, 32, 429, doi: [10.1086/190404](https://doi.org/10.1086/190404)
- Sundqvist, J. O., & Owocki, S. P. 2013, *MNRAS*, 428, 1837, doi: [10.1093/mnras/sts165](https://doi.org/10.1093/mnras/sts165)
- Sundqvist, J. O., Owocki, S. P., & Puls, J. 2018, *A&A*, 611, A17, doi: [10.1051/0004-6361/201731718](https://doi.org/10.1051/0004-6361/201731718)
- Sundqvist, J. O., & Puls, J. 2018, *A&A*, 619, A59, doi: [10.1051/0004-6361/201832993](https://doi.org/10.1051/0004-6361/201832993)
- ud-Doula, A., & Owocki, S. P. 2002, *ApJ*, 576, 413, doi: [10.1086/341543](https://doi.org/10.1086/341543)
- Underhill, A. B. 1975, *ApJ*, 199, 691, doi: [10.1086/153738](https://doi.org/10.1086/153738)
- Vink, J. S., de Koter, A., & Lamers, H. J. G. L. M. 2001, *A&A*, 369, 574, doi: [10.1051/0004-6361:20010127](https://doi.org/10.1051/0004-6361:20010127)
- Šurlan, B., Hamann, W. R., Aret, A., et al. 2013, *A&A*, 559, A130, doi: [10.1051/0004-6361/201322390](https://doi.org/10.1051/0004-6361/201322390)